

Quasi-simultaneous optical coherence tomography and confocal imaging

Irina Trifanov
Michael Hughes
Adrian Gh. Podoleanu
University of Kent
School of Physical Sciences
Applied Optics Group
Canterbury, CT2 7NH
United Kingdom

Richard B. Rosen
Advanced Retinal Imaging Center
New York Eye and Ear Infirmary
New York, New York 10003
and
New York Medical College
Valhalla, New York 10595

Abstract. A new approach of acquiring quasi-simultaneous optical coherence tomography (OCT) and confocal images is presented. The two images are generated using different principles, OCT and confocal microscopy. When the system is used to image the retina, the two images have depth resolutions, at present, of $<20\ \mu\text{m}$ and $\sim 1\ \text{mm}$, respectively. The acquisition and display of *en face* OCT and confocal images are quasi-simultaneous, without the need of a beamsplitter. By using a chopper to periodically obstruct the reference beam in the OCT interferometer, synchronized with the XY-transversal scanner, much higher acquisition speed is obtained than in a previous report where we flipped an opaque screen in the reference arm of the interferometer. Successful operation of the novel configuration was achieved by: (1) stable synchronization of the chopper's movement with the horizontal line scanner and (2) fast self-adjusting of the gain value of avalanche photodiodes, depending on the optical power. Images from coin, leaves, and retina *in vivo* have been collected to demonstrate the functionality of the system. © 2008 Society of Photo-Optical Instrumentation Engineers. [DOI: 10.1117/1.2957051]

Keywords: optical coherence tomography; scanning laser ophthalmoscopy; confocal microscopy; retina imaging.

Paper 07495R received Dec. 20, 2007; revised manuscript received Mar. 11, 2008; accepted for publication Mar. 11, 2008; published online Jul. 18, 2008.

1 Introduction

Any optical coherence tomography (OCT) configuration¹ is assembled around a confocal microscopy (CM) interface. Combining the two imaging technologies, CM and OCT, is especially useful when the orientation of images is *en face*. *En face* images or C-scans are slices of tissue oriented perpendicular to the optic axis. This is the orientation of choice in microscopy. CM was the first high-resolution imaging technology applied to the eye. The *en face* is also the orientation of choice of a confocal scanning laser ophthalmoscope (SLO).² Providing pixel-to-pixel correspondence *en face* CM (or SLO) and OCT images are useful for several reasons, such as guidance, precise on-line focusing,³ alignment and processing of the stack of OCT *en face* images prior to the construction of the three-dimensional (3D) data of the volume investigated.^{4,5} There are other reasons, too, such as complementarity of information and of presentation. Because of the high sectioning capability of the *en face* OCT, images look fragmented⁶ and may be difficult to interpret. Also, the confocal image is speckle free while the OCT image presents not only speckle, but extra noise due to the interference process and the excess photon noise,^{7,8} due to the low coherence properties of the optical source.

Generation of an SLO-like image of the eye has been found useful in OCT cross-sectional imaging as well. Several groups have reported inference of an SLO-like image from

B-scans using Fourier domain (channeled spectrum) OCT systems⁹ or swept source OCT.¹⁰

The two images could be acquired: (i) either simultaneously (a beamsplitter is needed for tapping into the signal backscattered from the sample)¹¹ or (ii) sequentially (an opaque screen is used for switching from one regime to the other).¹² The first implementation has a major disadvantage in terms of lowering the sensitivity of the OCT channel if the beamsplitter is placed between the object imaged and the interferometer aperture. The beamsplitter can also be placed between the source and the interferometer,^{4,13} but this requires a slightly higher power optical source and careful elimination of all stray reflections in the interferometer; the second implementation is time consuming and, therefore, suitable for imaging static objects only and less helpful for *in vivo* imaging.

However, the second solution employs the confocal core of the configuration and presents advantages in terms of lower complexity and a lower cost imaging system with lower optical losses, where all signals returned from the object are employed to produce a confocal image. In this paper, we report on such an optical configuration. Quasi-simultaneous imaging in the two regimes, OCT and CM, is achieved by using a chopper (instead of the opaque screen), which is controlled via a synchronization mechanism. This allows line-by-line operation, with a fast switching on the fly between the two regimes of operation, during the raster line of a dual-frame image. The sensitivity of the OCT channel is not lowered because no splitter is required. An additional difficulty was

Address all correspondence to: Irina Trifanov, University of Kent, School of Physical Sciences, Applied Optics Group, Canterbury, CT27NH, United Kingdom. E-mail: I.Trifanov@kent.ac.uk

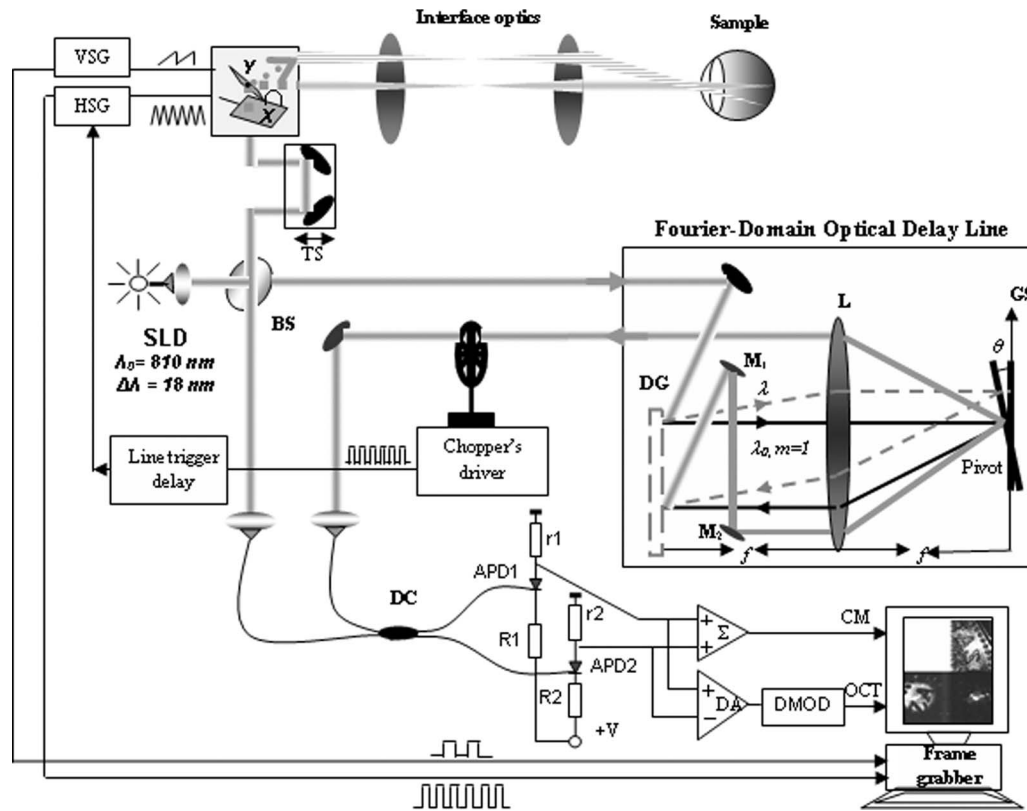


Fig. 1 Schematic diagram of the system. SLD, superluminescent diode (Superlum 361); BS, beamsplitter; DC, broadband directional coupler; DG, diffraction grating; M_1 , M_2 , mirrors; GS, galvanoscanner mirror; APD_{1,2} avalanche photodetectors; VSG, vertical signal generator; HSG, horizontal signal generator; Σ , summing amplifier; DA, differential amplifier; DMOD, demodulator block; $R_{1,2}$, ballast resistors; and $r_{1,2}$ determine the sensitivity of the photodetection.

raised by the need to employ avalanche photodetectors (APD) in order to achieve a sufficient signal-to-noise ratio in the CM channel. Low-noise electronics and optimization of APD voltage combined with the optical power level in the reference beam lead to a signal-to-noise ratio in the OCT regime close to that achieved when using PIN (p-type, intrinsic, n-type) photodetectors.

2 Experimental Configuration

The system, as shown in Fig. 1, is based on a two-splitter low-coherence hybrid interferometer optimized for broad bandwidth sources. Light from a superluminescent diode [(SLD), Superlum, Moscow] centered at 810 nm with an 18 nm bandwidth is launched into the system through a single-mode optical fiber port and then is split by a plate beamsplitter into an object and reference arm. The returned light from both arms is then routed into a second splitter, a broadband single-mode directional coupler. In the object arm of the interferometer, a pair of XY galvanometer scanners is employed to direct the beam via the interface optics to the object. The use of a hybrid OCT configuration, with one splitter in bulk,¹² is essential in eliminating the reflections in the object arm, which otherwise, when the reference beam is blocked, could still obscure the weak signal returned by the sample to be used in the CM channel.

A Fourier domain-optical delay line scheme in the reference arm is employed for dispersion compensation and depth

scanning. This works in transmission and exhibits low losses by traversing the diffraction grating (DG) only twice.¹⁴ The delay line uses a DG, an achromat lens (L) and a galvanometer scanner (GS) in a $2f$ configuration. The DG disperses a collimated beam, which is then imaged by L at a distance f away. The pivot of the GS, located in the other focal plane of L, causes a linear phase ramp on the spectrum and redirects the rays back to the DG through L. Here the spectrum is recombined into a collimated beam. The outgoing beam exits the DG at a different point, O, parallel to the incoming beam. The amount of mirror tilt, θ , translates into a group delay for the output beam. This is based on the well-known property of the Fourier theorem that a linear phase in frequency domain corresponds to a group delay in time domain. To eliminate the walk-off, mirrors M_1 and M_2 are used to send the recombined beam back to GS, where the angular tilt is descanned.

A chopper (SR540, Stanford Research Systems) is used to square-wave modulate the intensity of the reference beam. The chopper is powered by an adjustable voltage power supply, which is set to rotate the chopper at a repetition frequency of 500 Hz. The transistor-transistor logic (TTL) pulses delivered by the chopper are then fed into a function synthesizer (8116A Pulse/Function Generator, 50 MHz, Hewlett Packard) that outputs a triangle waveform at 500 Hz to drive the line scanner. Mechanical and electric delays in the scanners require adjustment of the correct timing when the reference beam is toggled on and off. A delay is introduced by the block

“line trigger delay” in the line delivering the TTL signal to the line frequency generator and this is adjusted as accordingly in order to synchronize the start of ray deflection over the object with the moment of toggling the reference beam power on and off. The chopper’s frequency was sufficiently stable not to require any adjustments during the imaging. The frame scanner in the XY pair is driven by a vertical signal generator with a sawtooth waveform at 1.5 Hz. The operation of the system is different on the two ramps of the triangle sent to the line scanner, a method reported before for generation of quasi-simultaneous OCT/OCT images with different depth resolutions.¹⁵

The system can be used to generate cross-sectional images by using either transverse priority or depth priority scanning and is suitable for compensating the dispersion when scanning in depth.¹⁶ However, for the present study, we used only transverse priority (*en face* imaging), where the carrier for the image bandwidth was created by the path modulation introduced by the galvoscaner determining the line in the final raster.^{17,18} Transversal priority OCT imaging was also reported using external phase modulation.¹⁹ The introduction of an electrooptic phase modulator into the low coherence interferometer raises the problem of dispersion compensation. We previously demonstrated that if the C-scan image is sufficiently wide²⁰ in terms of lines scanning, then there is no need for external phase modulation with the advantage of simplicity and cost. The utility and challenges of interpreting the C-scan OCT images of the retina as well as the advantages of simultaneous OCT and SLO acquisition have been previously evaluated for a variety of eye pathologies.³

The detection unit employs two avalanche photodetectors, APD1 and APD2 (Mitsubishi PD1002). Essential for the operation regime here is their self-switching,²¹ depending on the optical power applied and the value of the ballast resistors, R_1 and R_2 . Therefore, we have designed a special amplifier board that has allowed adjustment of the ballast resistor values and of the transimpedance in order to optimize the S/N ratio.

The CM signal is provided by the summing amplifier (Σ), where the two photodetected signals collected from $r1$ and $r2$ are added up. The OCT signal is available at the output of the difference amplifier after demodulation in the demodulator block. A dual-channel variable frame grabber (Bit flow, Raven) is used to display the two images.

The switching regime is illustrated in Fig. 2(a). Ideally, during the first half ramp of 1 ms (ascending slope), the reference beam is on and the system provides the OCT signal (while the CM channel is saturated). During the second half ramp of 1 ms (descending slope), the reference beam is blocked and the confocal signal is displayed (while the OCT channel provides a distorted CM image). For every line of 2 ms in the raster, 1 ms corresponds to one regime and the next to the other regime of operation. In practice, there is a delay between the signal applied to the transversal scanner and the actual galvomirror tilt, as well as other delays in the electronics circuitry, which requires correction via the “line trigger delay.” The OCT and SLO images captured by the system are mirror inverted with respect to the median of the frame-grabber display window.

3 Regimes of Operation

Depending on the reference optical power relative to the voltage drop on the ballast resistors, R , two possibilities exist:

1. Low reference power ($\sim 3 \mu\text{W}$). In this case, the reference power is just sufficient to generate a good OCT signal and the dc values sent to the confocal amplifier are insufficient to saturate it. This allows both channels OCT and confocal to operate while the reference beam is on. Figure 2(b) shows the confocal image of a coin on the left, while the reference beam is on. This is simultaneous with the OCT image at the bottom. However, there is noise due to the fluctuations of the SLD source power. Also, in order to achieve simultaneous display of the two images, the low strength of the reference beam power leads to poor quality of the OCT image too.

2. High reference power ($\sim 100 \mu\text{W}$). This is the preferred mode of operation. In this case, the confocal (SLO) amplifier is saturated, which does not allow for the tiny confocal signal to be noticed, and the confocal image is white, as shown in Fig. 2(c).

All subsequent images have been acquired with sufficient high power in the reference beam, which allows the OCT to exhibit high sensitivity. Because the CM is saturated when the reference is on and the OCT channel produces a distorted confocal image when the reference beam is off, they have been eliminated in all subsequent images shown. Only the useful parts of the images denoted as (1) and (2) in Figs. 2(b) and 2(c), have been cropped out of the dual panels and displayed in Figs. 3–5 below. The sectors eliminated are in white or black and correspond to the stray OCT images in the confocal regime and to the stray confocal images in the OCT regime.

Because the optical power incident on the APDs is different for the two regimes of operation, there are two related issues that require attention: (1) optimization of the APD bias circuit to achieve a good signal-to-noise ratio (SNR) in the confocal regime, when the APD works with high gain, close to the avalanche, and (2) minimization of the transit time required for the APD and subsequent electronics to self-switch from one regime to the other.

APDs differ from PIN photodiodes by providing internal photoelectronic signal amplification. However, the gain mechanism itself introduces noise, which depends on how close the voltage applied is to the avalanche voltage threshold. The APDs and the subsequent amplifier could have bandwidths in excess of tens of megahertz, and therefore, the switching regime of operation could be performed very quickly. Switching the power on and off in the reference path determines swings of several volts at the inputs of the APD amplifiers in the two channels. These swings are transferred to the confocal amplifier circuit, which is dc coupled; therefore, the signal at the confocal output will follow the transit in a time determined by the low-pass filter equivalent to the dc-coupled CM amplifier. There is also a transit time of the chopper edge through the beam, and this extends the time the CM image stays saturated after the chopper edge starts intercepting the reference beam.

On the other hand, the amplifier in the OCT is ac coupled and designed to transfer the image bandwidth created by path modulation. Therefore, we have optimized the time constant

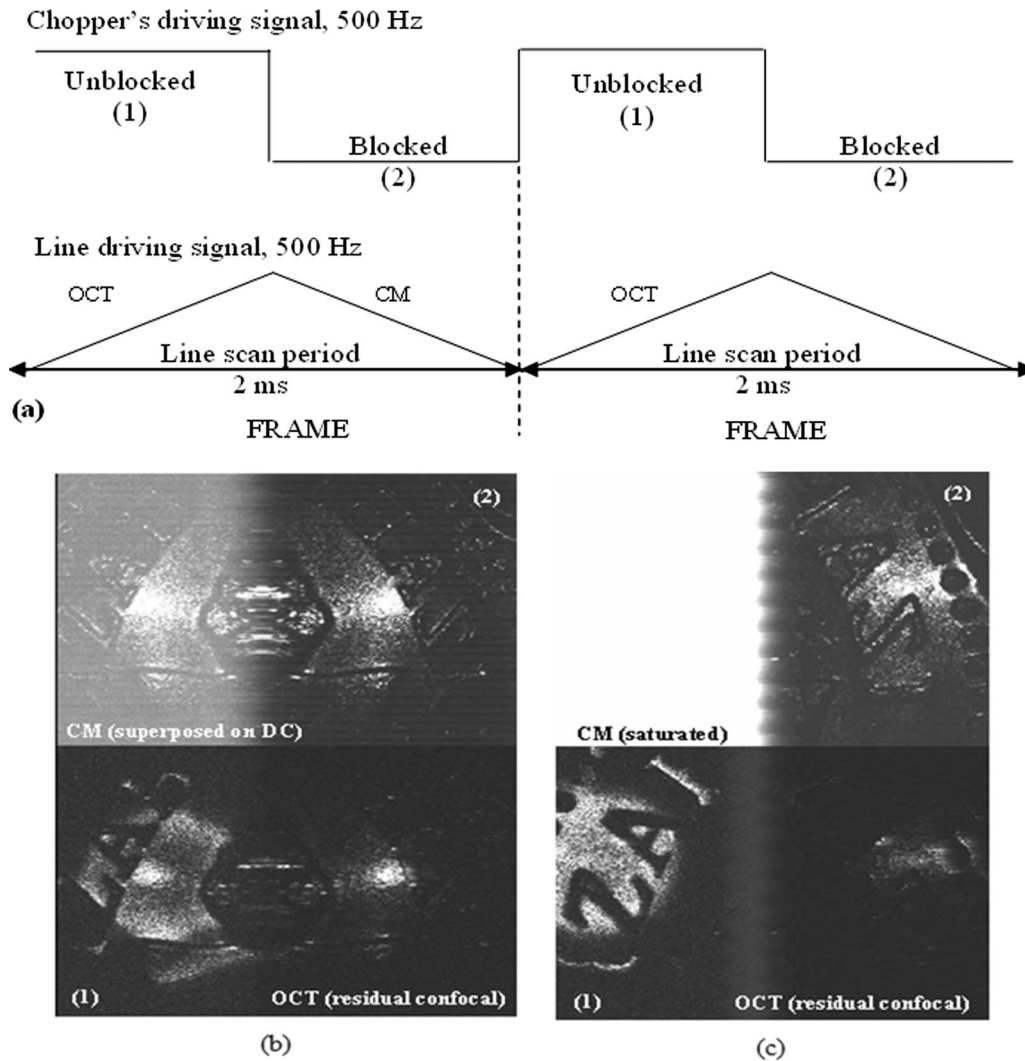


Fig. 2 (a) Driving signals. (b), (c) Pairs of *en face* quasi-simultaneous CM (top)—OCT (bottom) image of a 5-pence coin for different reference powers. Lateral image size: 2 mm (horizontal) \times 3 mm (vertical). The fly-back corresponding to the switch between the CM and OCT regime is visible in the middle of the images. The display is switched on after some time from the moment of CM to OCT switch to eliminate the ringings in the OCT image. This results in clipping the OCT image. Similarly, the CM image is also clipped due to the extension of saturation beyond the moment when the chopper starts intercepting the reference beam.

of the high-pass filter between the APDs and the OCT amplifier to reduce the extension of ringings in the OCT image immediately after the reference power was switched on. The ringings were also minimized by precise adjustment of the balance of photodetecting currents.

However, some residual switching effects remained, resulting in individual image edges being compromised. Therefore, the left-hand side of the compound images have been removed (this side corresponds to the switch between SLO and OCT, which was largely affected by ringings). A similar switching effect, combined with the fly back (i.e., where the scanning is nonlinear) is seen in the middle of the image in Fig. 2(c) bottom and such parts have also been removed from subsequent images. In addition, extension of white is noted within the confocal image in the top image in Fig. 2(c), beyond the moment of switching from OCT to SLO (reaching the letter “I”). In subsequent images, we cropped the CM

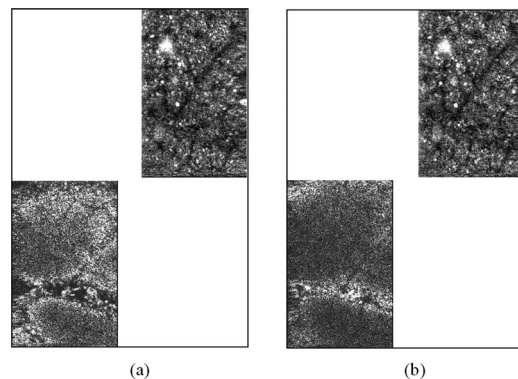


Fig. 3 Pairs of *en face* quasi-simultaneous confocal (top)—OCT (bottom) images from a leaf at different depths; (a) z_1 , (b) $z_2 = z_1 + 400 \mu\text{m}$. Lateral size: 2 mm (horizontal) \times 3 mm (vertical). The images here have been cropped from the originals and left in the same position with the OCT images horizontally reverted.

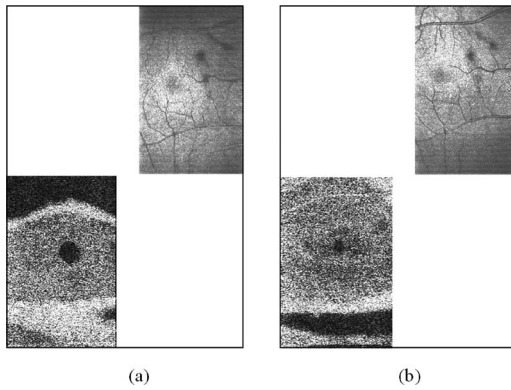


Fig. 4 Pairs of *en face* quasi-simultaneous confocal (top)–OCT (bottom) images of the fovea *in vivo* at different depths. Image size: 4 mm (horizontal) \times 7.5 mm (vertical). The images here have been cropped from the originals and left in the same position with the OCT images horizontally reverted.

(SLO) image at the border between the saturation and the image.

The lost part of the OCT image, after horizontal reversion, corresponds to its right-hand side while the CM image loses some of its left-hand side. Because image parts are eliminated from opposite sides of the two images after reverting one of them, the final two images look slightly different. We preferred not to eliminate parts from either of the images, which after cropping are left with no correspondence in the other. This does not mean that the pixel-to-pixel correspondence is compromised; this is maintained in the common parts of the two images.

This problem is not characteristic for the method implemented here. Better electronics circuitry can be devised to reduce the amount of voltage swing due to the obstruction of the beam. An electronic clipper can be used to limit the swing in conjunction with a specialized APD power supply, which delivers different voltage values depending on the regime of operation to further diminish the voltage swing, which propagates toward the image.

Figure 3 displays quasi-simultaneous OCT/CM images acquired from a leaf for two depth positions in the OCT chan-

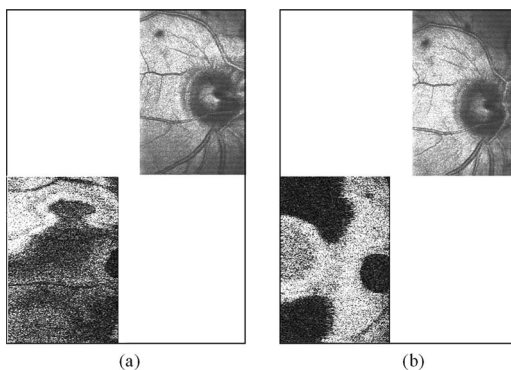


Fig. 5 Pairs of *en face* quasi-simultaneous confocal (top)–OCT (bottom) images of the optic nerve *in vivo* at different depths. Image size: 4 mm (horizontal) \times 7.5 mm (vertical). The images here have been cropped from the originals and left in the same position with the OCT images horizontally reverted.

nel. The CM channel provides a reference for the OCT exploration while scanning in depth. Clear distinction of cells is performed in the CM channel, which is essentially speckle free. Selection in depth and higher depth resolution is provided by the OCT channel, illustrating the benefits of the dual *en face* display of the two images. The images here have been cropped from the originals and left in the same position with the OCT images horizontally reverted. The same procedure was employed for the images in Figs. 4 and 5.

Figures 4 and 5 present images acquired from the eye of a volunteer (AP). In this case, the CM channel operates like a SLO instrument. We evaluated a FWHM of ~ 1 mm for the confocal profile in depth, as determined by the single-mode fiber aperture²² for a model eye made from a mirror behind a 2-cm focal achromat.

Quasi simultaneous OCT/SLO images of the fovea are presented in Fig. 4. The foveal pit is well resolved in the OCT images.

The images in Fig. 5 show the optic nerve of the volunteer. No bite bar was used; therefore, images show the effect of movement in the OCT *en face* images, which are more sensitive to movement distortion than the SLO images due to their thinner thickness. Different depth positions are shown in Figs. 4 and 5 obtained by controlling the translation stage in the object arm.

B-scan images could also be obtained, but the SLO image does not present any information. However, if dynamic focus was introduced, then the B-scan image in the SLO channel, especially when imaging the optic nerve, may have relevance.¹³

4 SNR Analysis and Optimization of the APD Circuit

In order to evaluate the SNR, an eye model was used, consisting of a piece of paper behind a 2-cm achromat lens. An optimization of the voltage applied to the APDs is required, because too low a voltage may prevent good amplification as required for the weak confocal channel and too large a voltage may be too close to the avalanche, which may lead to noise in both regimes.

The SNR for each regime of operation as a function of reverse bias voltage applied to the APDs was measured and results are presented in Fig. 6. The voltage is that of the power supply. The voltage on the APDs depends on the ballast resistors, R , and the reference power in the OCT regime. The noise in the CM regime does not depend on the reference power; this exclusively depends on how close the APD voltage is to the avalanche and on the electronics circuit noise. We investigated different sets of APDs (Mitsubishi) having different values for the ballast resistance. If the ballast resistor is too small, for instance below tens of kilohms, then power in excess of 100 μ W is required to switch the operation regime of APDs. In addition, if the resistance is too small, then when illuminated, the photocurrent may exceed the maximum limiting current and the APDs are destroyed. Therefore, in order to switch them, resistance values in excess of 50 k Ω were found suitable. Larger values may reduce the switching time due to the stray capacitances in the electronics and cables. When the APD voltage is below the avalanche, the APDs behave like pin diodes, with low gain and low noise. For

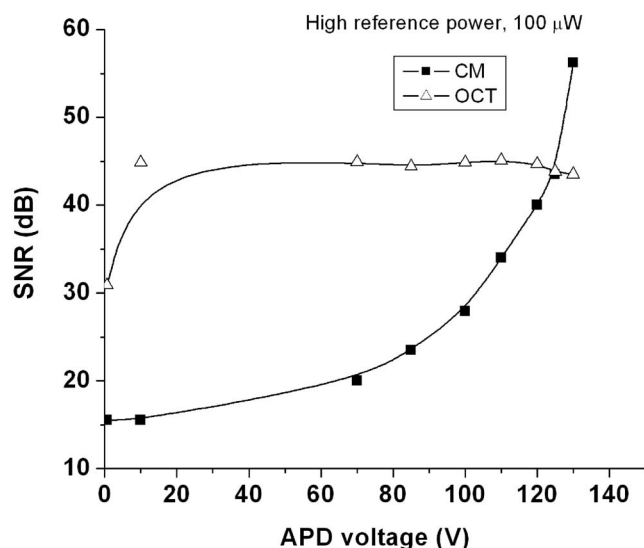


Fig. 6 The SNR as a function of the voltage applied, V (in Fig. 1) on the APDs for the case of high reference power in the confocal regime (\blacksquare) and in the OCT regime (\blacktriangle).

instance, for $R=200\text{ k}\Omega$, $100\text{ }\mu\text{W}$ was sufficient to switch the APDs to the low amplification regime and low noise was obtained as required for the OCT.

Figure 6 shows the S/N ratio in both channels as a function of the reverse bias. There is an optimum value ($\sim 120\text{ V}$) for the voltage applied to the APD block for which both channels exhibit “simultaneously” good SNR. However, the optimum SNR differs in each channel due to different noise terms in each regime of operation. This was the voltage utilized in obtaining the images in Figs. 3–5.

The noise depends on the bandwidth of the electronic chain following the APDs. Therefore, it has to be restricted to the minimum required to process the image bandwidth, which in our case is $\sim 150\text{ kHz}$, given by the number of pixels, in both channels. The high-pass filter to the OCT amplifier was set on 10 kHz to reduce the time taken by the charge accumulated in the capacitors to discharge, which obscures the OCT image.

The SNR obtained in the best combination of parameters was comparable to that using a Nirvana New Focus photodetector 2007 unit, which employs two pin photodetectors. When the bandwidth was restricted to 125 kHz (that of the Nirvana photodetector), the SNR obtained from a paper object was only 3 dB less by using the APD balanced receiver than using the Nirvana.

5 Conclusions

A solution was demonstrated for quasi-simultaneously imaging in two regimes, OCT and confocal. We have proven that a line-by-line operation is possible using a synchronous switching of the power in the reference arm of the interferometer with that of the lateral scanning. Optimization of the electronics circuitry following the APDs and their self-switching mechanism allowed good quality images to be obtained in both channels, toggled at 500 Hz .

Images have been collected from a coin, leaf, and the retina of a volunteer, proving the configuration applicability as an OCT/SLO dual system. The solution could easily be extended to the case where a resonant transversal scanner is employed, obviously with a corresponding increase in the bandwidth of the switching circuits, electronics, and imaging channels.

The main advantage of the configuration proposed is its simplicity. Elimination of the need for a beamsplitter to divert light to a confocal receiver leads to less problems in the dispersion management. Also, the optics adjustment demands are less than in any OCT/CM or OCT/SLO configurations, which require superposition of the optical axes of the two channels, OCT and CM (SLO). Here, once the focus adjustment is performed in the OCT, it is already achieved in the CM (SLO). We are now investigating the same configuration suitability for an OCT/adaptive optics combined system, where the object beam is already weekend by the high number of optical components. Using the principle illustrated, the same object arm path, corrected for aberrations, is sequentially used for OCT and for CM (SLO).

One drawback of the method presented is the effect of electronic switching on the images, which leads to some edge clipping. This also demands careful interpretation of pixel-to-pixel correspondence between the two images. Better electronics can reduce the areas of images affected by the regime switching.

The technical solution presented here to generate a CM (SLO) signal without resorting to a beamsplitter is equally applicable to a saw-tooth excitation of the transverse line scanner or for scanning instruments using polygon mirrors. In this case, toggling of the two regimes is implemented on alternative lines instead on the returning lines as presented here. This may have the advantage of eliminating the need to revert one of the images and can improve the pixel-to-pixel correspondence between the images because the electronic switching affects the same edge of the two images.

Acknowledgments

I. Trifanov acknowledges the Marie Curie training site grant supported by the European Commission, 2005-020353. M. Hughes acknowledges the support of the Leverhulme Trust UK. The authors acknowledge the technical support of Dr. Carla Rosa, University of Porto, Portugal, and of Dr. Radu Cucu, University of Kent, in setting the scanning delay line.

References

1. A. F. Fercher, “Optical coherence tomography,” *J. Biomed. Opt.* **1**(2), 157–173 (1996).
2. R. H. Webb, G. W. Hughes, and F. C. Delori, “Confocal scanning laser ophthalmoscope,” *Appl. Opt.* **26**, 1492–1499 (1987).
3. A. G. Podoleanu, G. M. Dobre, R. G. Cucu, R. Rosen, P. Garcia, J. Nieto, D. Will, R. Gentile, T. Muldoon, J. Walsh, L. A. Yannuzzi, Y. Fisher, D. Orlock, R. Weitz, J. A. Rogers, S. Dunne, and A. Boxer, “Combined multiplanar optical coherence tomography and confocal scanning ophthalmoscopy,” *J. Biomed. Opt.* **9**, 86–93 (2004).
4. A. M. Pircher, B. Baumann, E. Götzinger, H. Sattmann, and C. K. Hitzenberger, “Simultaneous SLO/OCT imaging of the human retina with axial eye motion correction,” *Opt. Express* **15**, 16922–16932 (2007).

5. B. M. Pircher, R. J. Zawadzki, J. W. Evans, J. S. Werner, and C. K. Hitzenberger, "Simultaneous imaging of human cone mosaic with adaptive optics enhanced scanning laser ophthalmoscopy and high-speed transversal scanning optical coherence tomography," *Opt. Lett.* **33**, 22–24 (2008).
6. A. G. Podoleanu, J. A. Rogers, and D. A. Jackson, "OCT *en face* images from the retina with adjustable depth resolution in real time," *IEEE J. Sel. Top. Quantum Electron.* **5**, 1176–1184 (1999).
7. K. Takada, "Noise in optical low-coherence reflectometry," *IEEE J. Quantum Electron.* **34**, 1098–1108 (1998).
8. A. G. Podoleanu and D. A. Jackson, "Noise analysis of a combined optical coherence tomograph and a confocal scanning ophthalmoscope," *Appl. Opt.* **38**, 2116–2127 (1999).
9. M. Wojtkowski, V. Srinivasan, J. G. Fujimoto, T. Ko, J. S. Schuman, A. Kowalczyk, and J. S. Duker, "Three dimensional retinal imaging with high-speed ultrahigh-resolution optical coherence tomography," *Ophthalmology* **112**, 1734–1746 (2005).
10. H. Lim, M. Mujat, C. Kerbage, E. C. Lee, Y. Chen, T. C. Chen, and J. F. de Boer, "High-speed imaging of human retina in vivo with swept-source optical coherence tomography," *Opt. Express* **14**, 12902–12908 (2006).
11. A. G. Podoleanu and D. A. Jackson, "Combined optical coherence tomograph and scanning laser ophthalmoscope," *Electron. Lett.* **34**(11), 1088–1090 (1998).
12. A. G. Podoleanu, G. M. Dobre, R. G. Cucu, and R. Rosen, "Sequential OCT and confocal imaging," *Opt. Lett.* **29**(4), 364–366 (2004).
13. M. Pircher, B. Baumann, E. Gotzinger, and C. K. Hitzenberger, "Retinal cone mosaic imaged with transverse scanning optical coherence tomography," *Opt. Lett.* **31**(12), 1821–1823 (2006).
14. C. C. Rosa, J. Rogers, and A. G. Podoleanu, "Fast scanning transmissive delay line for optical coherence tomography," *Opt. Lett.* **24**, 3263–3265 (2005).
15. A. G. Podoleanu, R. G. Cucu, R. B. Rosen, G. M. Dobre, J. A. Rogers, and D. A. Jackson, "Quasi-simultaneous OCT *en face* imaging with two different depth resolutions," *J. Phys. D* **36**, 1696–1702 (2003).
16. C. C. Rosa, J. Rogers, J. Pedro, R. Rosen, and A. G. Podoleanu, "Multiscan time-domain optical coherence tomography for retina imaging," *Appl. Opt.* **46**(10), 1795–1808 (2007).
17. A. G. Podoleanu, G. M. Dobre, D. J. Webb, and D. A. Jackson, "Coherence imaging by use of a Newton rings sampling function," *Opt. Lett.* **21**, 1789–1791 (1996).
18. A. G. Podoleanu, G. M. Dobre, D. J. Webb, and D. A. Jackson, "En face coherence imaging using galvanometer scanner modulation," *Opt. Lett.* **23**, 147–149 (1998).
19. C. K. Hitzenberger, P. Trost, P. Lo, and Q. Zhou, "Three-dimensional imaging of the human retina by high-speed optical coherence tomography," *Opt. Express* **11**, 2753–2761 (2003).
20. A. G. Podoleanu, M. Seeger, G. M. Dobre, D. J. Webb, D. A. Jackson, and F. W. Fitzke, "Transversal and longitudinal images from the retina of the living eye using low coherence reflectometry," *J. Biomed. Opt.* **3**, 12–20 (1998).
21. R. Cernat and A. Podoleanu, "Avalanche photodiode based optical coherence tomography," *Proc. SPIE* **5459**, 185–191 (2004).
22. S. Kimura and T. Wilson, "Confocal scanning optical microscope using single-mode fiber for signal detection," *Appl. Opt.* **30**, 2143–2150 (1991).